Measurement of the Inelastic Proton-Proton Cross-Section at $\sqrt{s} = 7$ TeV with the ATLAS Detector

A first measurement of the inelastic cross-section is presented for proton-proton collisions at a center of mass energy $\sqrt{s} = 7$ TeV using the ATLAS detector at the Large Hadron Collider. In a dataset corresponding to an integrated luminosity of 20 μb^{-1}, events are selected by requiring hits on scintillation counters mounted in the forward region of the detector. An inelastic cross-section of 60.3 ± 2.1 mb is measured for $\xi > 5 \times 10^{-6}$, where $\xi = M_X^2/s$ is calculated from the invariant mass, M_X, of hadrons selected using the largest rapidity gap in the event. For diffractive events this corresponds to requiring at least one of the dissociation masses to be larger than 15.7 GeV.

Since the earliest days of particle physics, measurements of the total pp and $p\bar{p}$ cross-sections and their theoretical understanding have been topics of much interest [1]. The cross-sections can not yet be calculated by quantum chromodynamics (QCD), and many approaches have been used to describe the existing measurements. General arguments based on unitarity, analyticity, and factorisation imply a bound (the Froissart bound [2, 3]) on the high-energy behaviour of total hadronic cross-sections. This bound is independent of the details of the strong interaction dynamics and states that the total cross-section can not rise faster than $\ln^2(s)$, where $\sqrt{s}$ is the centre-of-mass energy. Recently it has been extended to the inelastic cross-section [4]. Existing experimental data [1] show a rise in the hadronic cross-sections with s, but it is unclear whether the asymptotic behaviour has already been reached. With the data presented in this letter we shed further light on the high energy behaviour of the inelastic cross-section.

The most common models that describe the data up to $\sqrt{s} = 1.8$ TeV predict a rise of the cross-section with a simple power law ($s^{\alpha(0)-1}$ where $\alpha(0)$ denotes the Pomeron-trajectory intercept) [5–7] or as a logarithm [8–11]. Others employ QCD for aspects of the calculation [12–14]. However, while the phenomenological description of the existing data is largely adequate, there are significant uncertainties on the extrapolation to higher energies, partly due to a long-standing 2.7σ discrepancy between the two highest energy collider measurements of the total $p\bar{p}$ cross-section by CDF [15] and by E811 [16].

In this letter a measurement of the inelastic pp cross-section is presented using data taken by the ATLAS experiment [17] at the Large Hadron Collider (LHC) [18] at $\sqrt{s} = 7$ TeV. The data considered were collected during a single 8-hour fill beginning March 31st, 2010, corresponding to an integrated luminosity of 20.3 ± 0.7 μb^{-1} and a peak instantaneous luminosity of 1.2×10^{27} cm^{-2}s^{-1}. The mean number of interactions per crossing in this fill is approximately 0.01. The analysis uses highly efficient scintillation counters to detect inelastic collisions. They are insensitive to diffractive dissociation processes in which the dissociation systems have small invariant masses, M_X. Their acceptance corresponds approximately to $\xi = M_X^2/s > 5 \times 10^{-6}$, equivalent to

$M_X > 15.7$ GeV for $\sqrt{s} = 7$ TeV. The cross-section measurement presented here is restricted to this kinematic range. However, in order to compare the data with previous measurements, an extrapolation of the cross-section is performed to the full ξ range, $\xi > m_p^2/s$ where m_p is the proton mass.

The ATLAS detector is described in detail elsewhere [17]. The beam-line is surrounded by a tracking detector that uses silicon pixel, silicon strip, and straw tube technologies and is embedded in a 2 T magnetic field. The tracking system covers the pseudorapidity [19] range $|\eta| < 2.5$. It is surrounded by electromagnetic and hadronic calorimeters covering $|\eta| < 3.2$, which are complemented by a forward hadronic calorimeter covering $3.1 < |\eta| < 4.9$. Minimum Bias Trigger Scintillator (MBTS) detectors, the primary detectors used in this measurement, are mounted in front of the endcap calorimeters on both sides of the interaction point at $z = \pm 3.56$ m and cover the range $2.09 < |\eta| < 3.84$. Each side consists of 16 independent counters divided into two rings; the inner 8 counters cover the rapidity range $2.83 < |\eta| < 3.84$ and the outer 8 counters cover the range $2.09 < |\eta| < 2.83$. Each individual counter spans 45° of the azimuthal angle (ϕ), and 31 out of 32 counters were operational. The luminosity is measured using a Cherenkov light detector, LUCID, which is located at $z = \pm 17$ m. The luminosity calibration has been determined during dedicated van der Meer beam scans to a precision of 3.4% [20, 21].

Monte Carlo (MC) simulations are used to determine the acceptance of the event selection and to assess systematic uncertainties. The detector response to the generated events is simulated using the ATLAS simulation [22] based on GEANT4 [23], and both the simulated and data events are reconstructed and analysed with the same software. The PYTHIA6 [24], PYTHIA8 [25] and PHOJET [26] generators are used to predict properties of inelastic collisions. These generators distinguish between different processes that contribute to inelastic pp interactions: *single dissociative* (SD) processes, $pp \rightarrow pX$, in which one proton dissociates; *double dissociative* (DD) processes, $pp \rightarrow XY$, in which both protons dissociate with no net color flow between the systems X and Y; and *non-diffractive* (ND) processes in which color flow is present between the two initial-state protons. The

model by Schuler and Sjöstrand [27], used by PYTHIA6 and PYTHIA8, predicts cross-sections of 48.5 mb, 13.7 mb and 9.3 mb for the ND, SD and DD processes, respectively. While the cross-sections used by PYTHIA6 and PYTHIA8 are identical, they differ in the modelling of the hadronic final state. PHOJET predicts the corresponding cross-sections as 61.6 mb (ND), 10.7 mb (SD) and 3.9 mb (DD). Due to differences in implementation of the interface between large ξ diffractive (SD and DD) processes and ND processes in PYTHIA and PHOJET the fractional contribution of these processes is a model dependent quantity. PHOJET also includes a 1.1 mb contribution from *central diffraction* (CD), $pp \rightarrow ppX$, a process not implemented in PYTHIA, wherein neither proton dissociates but the Pomeron-trajectory exchange results in energy loss for the protons and the production of a central system of particles. The MC generators define the inelastic cross-section as the sum of these contributions, and thus Schuler and Sjöstrand (PHOJET) predicts an inelastic cross-section of 71.5 mb (77.3 mb). Other recent predictions for this cross-section at $\sqrt{s} = 7$ TeV are 69 mb [10], 65-67 mb [12], 68 mb [13] and 60-75 mb [14].

The variable ξ is defined at the particle level by dividing the final state particles into two systems, X and Y. The mean η of the two particles separated by the largest pseudorapidity gap in the event is used to assign all particles with greater pseudorapidity to one system and all particles with smaller pseudorapidity to the other [28]. The mass, $M_{X,Y}$, of each system is calculated and the higher mass system is defined as X while the lower mass system is defined as Y. The variable ξ is then given by $\xi = M_X^2/s$ and it is bounded by the elastic limit of $\xi > m_p^2/s$. Due to the limited MBTS detector acceptance in η, this measurement is restricted to the range $\xi > 5 \times 10^{-6}$; there is no restriction on M_Y. Several models are used for the dependence of the diffractive cross-sections on ξ. The Schuler and Sjöstrand model has a relatively flat dependence on ξ, while the PHOJET model predicts a slight decrease with decreasing ξ. PYTHIA8 has several additional predictions for the ξ-dependence of the diffractive cross-sections which are considered. Bruni and Ingelman [29] predict a flat ξ-dependence while Donnachie and Landshoff (DL) [30], Berger *et al.* [31], and Streng [32] predict

$$\frac{\mathrm{d}\sigma_{SD}}{\mathrm{d}\xi} \propto \frac{1}{\xi^{1+\epsilon}}\,(1+\xi)$$

where $\epsilon = \alpha(0) - 1$. Values of ϵ between 0.06 and 0.10, and of α' between 0.10 and 0.40 GeV^{-2} are considered for the DL model. α' is the slope of the Pomeron trajectory which is assumed to be linear such that $\alpha(t) = \alpha(0) + \alpha't$. The DL model with $\epsilon = 0.085$ and $\alpha' = 0.25$ GeV^{-2} with PYTHIA8 fragmentation is the default model in this analysis and the other models are used to assess uncertainties in the modelling of diffractive events.

Experimentally the cross-section is calculated using

$$\sigma_{inel}(\xi > 5 \times 10^{-6}) = \frac{(N - N_{BG})}{\epsilon_{trig} \times \int L\mathrm{d}t} \times \frac{1 - f_{\xi < 5 \times 10^{-6}}}{\epsilon_{sel}}$$

where N is the number of selected events, N_{BG} is the number of background events, $f_{\xi < 5 \times 10^{-6}}$ is the fraction of events that pass the event selection but have $\xi < 5 \times 10^{-6}$, $\int L\mathrm{d}t$ is the integrated luminosity, and ϵ_{trig} and ϵ_{sel} are the trigger and offline event selection efficiencies in the selected ξ-range. Note that in this analysis ξ is defined only at the particle level; the cut value at 5×10^{-6} was chosen such that the efficiency of the MBTS requirement is greater than 50% for any ξ-values greater than 5×10^{-6}. In this measurement N_{BG} and ϵ_{trig} are determined directly from the data. The MBTS individual counter efficiencies in the MC simulation are tuned to match the observed efficiencies in data. Then ϵ_{sel} and $f_{\xi < 5 \times 10^{-6}}$ are taken from the tuned MC simulation. In order to reduce the uncertainties in the factors taken from MC simulation, the relative diffractive dissociation cross-section, $f_D = \frac{\sigma_{SD} + \sigma_{DD} + \sigma_{CD}}{\sigma_{inel}}$ for each generator is constrained. Each of these steps is described in detail below.

The MBTS functions as a trigger by determining the number of scintillation counters with a signal passing a leading-edge discriminator; in this analysis at least one trigger signal must be present. In the offline reconstruction, the MBTS signals are fit to obtain the total charge and timing of the signal. The offline event selection requires at least two counters with a charge larger than 0.15 pC. This threshold is set to be well above the noise level, which is well described by a Gaussian centred at zero of width 0.02 pC. This *inclusive* sample contains 1,220,743 data events. In order to constrain the diffractive components a subset of events is selected, the *single-sided* sample, which contains events that have at least two hits on one side of the MBTS detector and no hits on the opposing side (in z). In the data 122,490 single-sided events are observed.

Backgrounds arise from beam-related interactions, such as collisions of the beam with gas particles in the beam-pipe or with material upstream from the detector, and slowly-decaying, collision-induced radiation termed "afterglow" [21]. Additionally, instrumental noise and cosmic rays provide backgrounds which were studied and found to be negligible for this analysis. The beam-related backgrounds are determined using the number of selected events collected in this fill with the non-colliding bunches, i.e. when only one proton bunch was passing through AT-LAS [33], normalised by the ratio of the number of protons in the colliding to the non-colliding bunches. The single-sided selection contains 422 ± 28 background events and the inclusive sample contains $N_{BG} = 1,574 \pm 54$ background events, corresponding to 0.3% and 0.1% of the total samples, respectively. In addition, there is an in-time afterglow component due to the scattering of secondary low-energy particles produced in the same collision event which can give additional hits, causing low-activity events to migrate into the selected event sample. This contribution is evaluated to be at most 0.4% for the inclusive, and 3.6% for the single-sided, samples by examining the asymmetry of the absolute timing measurement of the MBTS counters. We conservatively assume

a 100% uncertainty on both background sources which covers any residual impact of the afterglow on the background subtraction, any uncertainty in the beam current measurements and the uncertainty due to in-time afterglow. The resulting overall uncertainty on the number of background events N_{BG} is given by the quadratic sum of the two components and is 0.4%.

The trigger efficiency of the MBTS detector with respect to the offline requirement, ϵ_{trig}, is measured to be $99.98^{+0.02}_{-0.12}\%$ (statistical errors) using events triggered randomly on colliding beams. The systematic uncertainty on ϵ_{trig} is determined using a second, independent trigger as reference. The difference between the two efficiency determinations leads to a 0.1% uncertainty on the cross-section measurement.

The data and MC simulation agreement in the MBTS counter response is checked using other detector subsystems with overlapping η ranges: charged particles reconstructed by the tracking detector ($2.09 < |\eta| < 2.5$), and calorimeter showers in the inner wheel of the electromagnetic calorimeter ($2.5 < |\eta| < 3.2$) and in the forward calorimeter ($3.1 < |\eta| < 3.84$). The efficiency with respect to a track (calorimeter energy deposit) to have a signal above the 0.15 pC threshold in the outer (inner) counters is on average 98.5% (97.5%) for the data and a constant 99.4% (98.7%) in the MC simulation. The individual counter efficiencies deviate by up to 2.0% (2.5%) from the average in the data. The MC simulation is corrected to match the data efficiency and the maximum variations in the counter responses are considered as a systematic uncertainty. This results in a 0.1% uncertainty on the cross-section measurement.

The offline selection efficiency, ϵ_{sel}, depends on the amount of material traversed by particles before hitting the MBTS detector. The rate of photons (primarily from π^0 decays) converting to electrons which are subsequently detected by the MBTS increases with additional material, resulting in an increase of ϵ_{sel}. Second order effects arise from charged particles scattering out of the MBTS acceptance region (decreasing ϵ_{sel}), or charged particles scattering into the acceptance region (increasing $f_{\xi<5\times10^{-6}}$). Within the tracking volume ($|\eta| < 2.5$) the material distribution has been studied using conversion electrons and $K_s^0 \to \pi^+\pi^-$ decays, and is known to better than $\pm5\%$ in the central region of the detector and to $\pm30\%$ for $2.2 < |\eta| < 2.5$ [33]. In the region $|\eta| > 2.5$ the material is dominated by the cooling and electrical services to the silicon pixel detector, and an uncertainty of $\pm40\%$ is assumed. This is validated *in-situ* using the fraction of events where we observe significant energy in the forward calorimeters but no signal (above noise) in the MBTS detector. The resulting systematic uncertainty on the cross-section is 0.2%.

Misalignments of the MBTS detector with respect to the nominal centre of the detector could change the event selection efficiency for a particular value of ξ. Misalignments of up to 10 mm were considered and found to have a negligible impact. A misalignment of 10 mm is conser-

vative compared to the survey precision and any known misalignments within the ATLAS experiment [17].

The fractional contribution of diffractive events, f_D, is constrained by the ratio of single-sided to inclusive events, R_{ss}. The MC generators predict that less than 1% of the ND process pass the single-sided event selection, while $27 - 41\%$ of the SD and DD processes pass the single-sided selection. For all models the inclusive sample is dominated by ND events, therefore the ratio of single-sided to inclusive events is sensitive to the relative fraction of diffractive events.

The measured R_{ss} in the data is $R_{ss} = [10.02 \pm 0.03(\text{stat.}) {}^{+0.1}_{-0.4}(\text{syst.})]\%$, where the systematic error includes the uncertainties on the backgrounds, the MBTS response and the material.
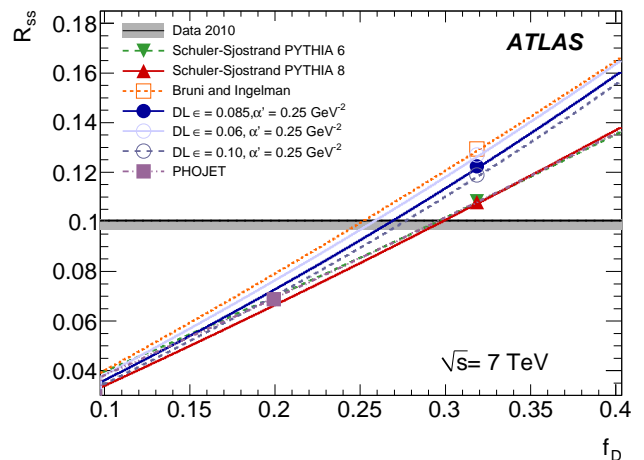

Figure 1: The ratio of the single-sided to inclusive event sample R_{ss} as a function of the fractional contribution of diffractive events to the inelastic cross-section f_D. The data value for R_{ss} is shown as the horizontal line with its systematic uncertainties (grey band). Also shown are predictions of several models as a function of an assumed value of f_D. The default f_D value (32.2% for all models but PHOJET which is 20.2%) is indicated by the markers.

Fig. 1 compares the observed value of R_{ss} to the predictions of several models as a function of f_D. The intersection of the R_{ss} value measured in data with the prediction is used as the central value of f_D for each model. The systematic uncertainty on f_D is determined by the maximum and minimum values consistent with the 1σ uncertainty on the data when varying the double- to single-dissociation event ratio between 0 and 1. The resulting value using the default DL model is $f_D = 26.9^{+2.5}_{-1.0}\%$.

The acceptance calculation relies on the MC generators to provide an adequate description of the particle multiplicity in the acceptance region. The validity of the MC description is assessed by examining the hit multiplicity in the MBTS detector in the inclusive and single-sided event samples as shown in Fig. 2. While none of the generators gives a perfect description, the data lie

between the models at low multiplicity which is most important for the measurement. The default DL model describes the single-sided sample well, giving confidence in the diffractive modelling. We use the difference in the MC correction factor determined with PYTHIA8 and PYTHIA6 as the uncertainty due to the fragmentation model, leading to a 0.4% uncertainty on the cross-section. The maximum difference between the default DL model and all other models is taken as the uncertainty due to the underlying ξ distribution. Variations of α' have a negligible effect on the acceptance. Among all the models considered, the PHOJET model gives the largest difference in the correction factor, leading to a 0.4% uncertainty on the cross-section.

Source	Uncertainty (%)
Trigger Efficiency	0.1
MBTS Response	0.1
Beam Background	0.4
f_D	0.3
MC Multiplicity	0.4
ξ-Distribution	0.4
Material	0.2
Luminosity	3.4
Total	3.5

Table I: Sources of systematic uncertainty and their effect on the cross-section measurement.

The final result for the measured inelastic cross-section is calculated using the default DL model of $\epsilon = 0.085$ and $\alpha' = 0.25$, which yields $f_D = 26.9\%$, $\epsilon_{sel} = 98.77\%$, and $f_{\xi<5\times10^{-6}} = 0.96\%$. Together with $\epsilon_{trig} = 99.98\%$, $N = 1,220,743$, $N_{BG} = 1,574$ and $\int L\mathrm{d}t = 20.25~\mu\mathrm{b}^{-1}$ this results in $\sigma_{inel}(\xi > 5 \times 10^{-6}) = 60.3 \pm 0.05(\mathrm{stat}) \pm 0.5(\mathrm{syst}) \pm 2.1(\mathrm{lumi})$ mb. The systematic uncertainty includes all contributions discussed above and listed in Table I; the dominant uncertainty arises from the luminosity calibration and is quoted separately.

The measurement is compared to the predictions in Figure 3 and Table II. The predictions by the Schuler-Sjöstrand model (66.4 mb) and the PHOJET model (74.2 mb) are both higher than the data. The prediction of 51.8-56.2 mb by Ryskin *et al.* [12] is slightly lower than the data.

In order to compare with previous measurements and analytic models, the fractional contribution to the inelastic cross-section of events passing the $\xi > 5 \times 10^{-6}$ cut is determined from the models and used to extrapolate the measurement to the full inelastic cross-section. This fraction is 87.3% for the default model of DL with $\epsilon = 0.085$ and $\alpha' = 0.25$. The other models considered give fractions ranging from 96%(PHOJET) to 86%(DL with $\epsilon = 0.10$). Recent calculations also yield values between 79% and 84% [12]. Thus 87% is taken as the default value for this fraction and an uncertainty of 10% is taken due to the extrapolation uncertainty on the ξ-dependence. The resulting inelastic cross-section value is $\sigma_{inel} = 69.4 \pm 2.4(\mathrm{exp.}) \pm 6.9(\mathrm{extr.})$ mb where exp includes the statistical and experimental systematic errors, including the luminosity uncertainty.

This result is shown in Fig. 3 compared to several theoretical predictions and a variety of data at lower $\sqrt{s}$. The measurement within the kinematic range $\xi > 5 \times 10^{-6}$ is significantly lower than the predictions of Schuler and Sjöstrand and PHOJET. The extrapolated value agrees within the large extrapolation uncertainty with the predictions from PYTHIA, which uses a power law dependence on $\sqrt{s}$. It also agrees with Block and Halzen [10] (which has a logarithmic $\sqrt{s}$ dependence), and with other recent theoretical predictions that vary between 60 and
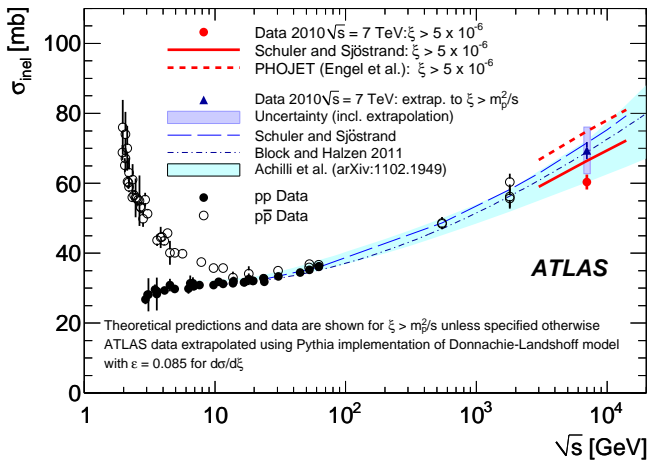

(a)

(b)

Figure 2: The MBTS multiplicity distribution in the data (filled circles) compared with MC expectations for the *inclusive* (a) and *single-sided* (b) samples for several MC models (histograms) using the fitted f_D values. The band around the data indicates the systematic uncertainty due to the MBTS detector response and the amount of material in front of the MBTS detector.

Figure 3: The inelastic cross-section versus $\sqrt{s}$. The ATLAS measurement for $\xi > 5 \times 10^{-6}$ is shown as the red filled circle and compared with the predictions of Schuler and Sjöstrand and PHOJET for the same phase space. Data (filled circles for pp data and unfilled circles for $p\bar{p}$ data) from several experiments are compared with the predictions of the pp inelastic cross-section from Schuler and Sjöstrand [27] (as used by PYTHIA), by Block and Halzen [10] and by Achilli *et al.* [14]. An extrapolation from the measured range of $\xi > 5 \times 10^{-6}$ to the full inelastic cross-section using the acceptance of $87 \pm 10\%$ is also shown (blue filled triangle). The experimental uncertainty is indicated by the error bar while the total (including the extrapolation uncertainty) is represented by the blue shaded area.

72 mb [12–14]. It should be stressed that this extrapolation relies on the prediction of the ξ-dependence of the cross-section.

The measurement and a variety of theoretical predictions are also summarised in Table II.

In conclusion, a first measurement of the inelastic cross-section has been presented for pp collisions at $\sqrt{s} = 7$ TeV with a precision of 3.5%. The measurement is limited to the kinematic range corresponding to the detector acceptance: $\xi > 5 \times 10^{-6}$. Phenomenological predictions for both a power law dependence and a logarithmic rise of the cross-section with energy are consistent with the measurement.

Acknowledgements

$\sigma(\xi > 5 \times 10^{-6})$ [mb]	
ATLAS Data 2010	60.33 ± 2.10(exp.)
Schuler and Sjöstrand	66.4
PHOJET	74.2
Ryskin *et al.*	$51.8 - 56.2$

$\sigma(\xi > m_p^2/s)$ [mb]	
ATLAS Data 2010	69.4 ± 2.4(exp.) ± 6.9(extr.)
Schuler and Sjöstrand	71.5
PHOJET	77.3
Block and Halzen	69
Ryskin *et al.*	$65.2 - 67.1$
Gotsman *et al.*	68
Achilli *et al.*	$60 - 75$

Table II: Measurement and theoretical predictions of the inelastic cross-section for the restricted kinematic range, $\xi > 5 \times 10^{-6}$, and for the full kinematic range, $\xi > m_p^2/s$. The experimental uncertainty (exp.) includes the statistical, systematic and luminosity uncertainties. The extrapolation uncertainty (extr.) only applies to the full kinematic range and is listed separately.

[1] K. Nakamura et al. (Particle Data Group), Chapter 41, pg.385-401, J. Phys. G **37** (2010) 075021. and references therein.

[2] M. Froissart, Phys. Rev. **3** 123 (1961) 1053-1057.

[3] A. Martin, Nuovo cimento **42** (1966) 930.

[4] A. Martin, Phys. Rev.D **80** (2009) 065013.

[5] P.D.B. Collins, *An introduction to Regge theory and high energy physics*, Cambridge University Press 1977, and references therein.

[6] A. Donnachie and P.V. Landshoff, Phys. Lett. B **296** (1992).

[7] A. Donnachie and P.V. Landshoff, Phys. Lett. B **595** (2004) 393.

[8] M.M. Block, K. Kang and A.R. White, Int. J. Mod. Phys **A7** (1992) 4449, and references therein.

[9] M. M. Block and R. N. Cahn, Rev. Mod. Phys. **57** (1985) 563; M. M. Block, Physics Reports **436** (2006) 71-215.

[10] M. M. Block and F. Halzen, arXiv:1102.3163.

[11] J. R. Cudell, K. Kang, S. K. Kim, Phys. Lett. B **395** (1997) 311-331.

[12] M. Ryskin, A. Martin, V. Khoze, arXiv:1102.2844, submitted to Eur. Phys. J. C.; private communication.

[13] E. Gotsman, E. Levin, U. Maor, J. S. Miller, Eur. Phys. J. C**57** (2008) 689-709; E. Gotsman, E. Levin, U. Maor, arXiv:1010.5323.

[14] A. Achilli *et al.*, CERN-PH-TH/2011-018, arXiv:1102.1949, submitted to JHEP.

[15] F. Abe *et al.* (CDF Collaboration), Phys. Rev. D **50** (1994) 5550-5561.

[16] C. Avila *et al.* (E811 Collaboration), Phys. Lett. B **445** (1999) 419-422.

[17] ATLAS Collaboration, JINST 3 (2008) S08003.

[18] L. Evans, (ed.), P. Bryant, (ed.), LHC Machine, JINST 3 (2008) S08001.

[19] ATLAS uses a right-handed coordinate system with its origin at the nominal interaction point (IP) in the centre of the detector and the z-axis coinciding with the axis of the beam pipe. The x-axis points from the IP to the centre of the LHC ring, and the y axis points upward. Cylindrical coordinates (r, ϕ) are used in the transverse plane, ϕ being the azimuthal angle around the beam pipe. The pseudorapidity is defined in terms of the polar angle θ as $\eta = -\ln \tan(\theta/2)$.

[20] S. van der Meer, CERN-ISR-PO-68-31, 1968.

[21] ATLAS Collaboration, ATLAS-CONF-2011-011; ATLAS Collaboration, arXiv:1101.2185v1, accepted by EPJC.

[22] ATLAS Collaboration, Eur. Phys. J. C**70** (2010) 823-874.

[23] S. Agostinelli, et al., GEANT4 Collaboration, GEANT4: A simulation toolkit, Nucl. Instr. Meth. A **506** (2003) 250303.

[24] PYTHIA version 6.421; T. Sjostrand, S. Mrenna, P. Skands, JHEP **05** (2006) 026.

[25] PYTHIA version 8.135; T. Sjostrand, S. Mrenna, P. Skands, Comput. Phys. Commun. **178** (2008) 852-867.

[26] R. Engel, Z. Phys. C **66** (1995) 203-214; R. Engel, J. Ranft, Phys. Rev. D **54** (1996) 4244-4262.

[27] G. Schuler and T. Sjöstrand, Phys. Rev. D **49** (1994) 2257-2267.

[28] C. Adloff *et al.* (H1 Collaboration), Z. Phys. C **74** (1997) 221.

[29] P. Bruni and G. Ingelman, Phys. Lett. B311 (1993) 317.

[30] A. Donnachie and P. V. Landshoff, Nucl. Phys. B244 (1984) 322.

[31] E. L. Berger et al., Nucl. Phys. B286 (1987) 704.

[32] K. Streng, CERN-TH.4949 (1988)

[33] ATLAS Collaboration, Phys. Lett. B **668** (2010) 1.